Mechanical properties of a carbon nanotube fixed at a tip apex: A frequency-modulated atomic force microscopy study

D. Dietzel,[1] S. Marsaudon,[1] J. P. Aimé,[1,*] C. V. Nguyen,[2] and G. Couturier[1]
[1]*CPMOH, Université Bordeaux 1, 351 cours de la libération F-33405 Talence Cedex, France*
[2]*NASA Ames Research Center, Moffet Field, California 94035, USA*
(Received 6 July 2004; revised manuscript received 11 January 2005; published 15 July 2005)

An investigation of mechanical properties of carbon nanotubes (CNTs) fixed at a tip apex was performed using a frequency modulation–atomic force microscope (FM-AFM). The FM-AFM method allows to measure conservative and nonconservative forces separately and unambiguously. The force gradient analysis provides a good understanding of the effects of the interaction between the free CNT end and the surface; the resonant frequency shifts provide information on the effective CNT spring constant, while the damping signal gives information on the sticking condition of the tube on the surface. Variation of the damping signal indicates that additional energy losses are mostly due to adhesion hysteresis. In particular, a close correlation between damping and resonant frequency shifts was observed. The whole variations show how the contact between the free CNT end and the surface modifies the elastic response of the tube and, in turn, the resonant frequency shift. Although not being quantitative, the cumulate variations of damping and resonance frequency provide a picture that is accurate enough to explain the effect for imaging and, in turn, find routes to enhance the contrast. An example is given with an image of InAs nanodots on GaAs.

DOI: 10.1103/PhysRevB.72.035445 PACS number(s): 68.37.−d, 68.65.−k, 07.79.−v

I. INTRODUCTION

In 1991, the discovery of carbon nanotubes[1] (CNTs) opened whole new fields of study in physics, chemistry, and material science. With diameters ranging from 1 to 100 nm and with lengths up to several millimeters,[2] carbon nanotubes possess a unique combination of nanometer and large-scale sizes. Additionally, they are characterized by high stiffness, high strength, and a broad range of electronic properties. Thus, the field of their applications is immense, e.g., high-strength fiber-reinforcing elements in composites, connecting components in nanoscale electronics, and ultrasharp and resistant atomic force microscope (AFM) tips with high aspect ratios.

From the structural point of view, CNTs can be divided into two distinct groups. Multiwalled carbon nanotubes (MWNT) consist of nested, concentric tubes. The interlayer spacing can range from 0.342 to 0.375 nm, depending on the number of shells comprising the tube.[3] For comparison, the interlayer spacing in graphite is 0.335 nm. The large interlayer spacing suggests a relatively weak interaction between individual shells, a fact that implies the broad range of mechanical and electronic properties of CNTs.

The second type of CNT is, in basic form, a rolled-up graphitic sheet, a single-walled CNT (SWNT). The diameter distribution of SWNTs is relatively narrow, thus they often bundle up in the form of crystalline "ropes,"[4] where the single tubes are held together by van der Waals interaction. Tubes inside the ropes can easily slide between them so that the ropes might have a weak shear modulus.

Therefore, whatever the production methods used, arc-discharge synthesis,[1,5] laser-ablation method,[4] or CVD growth,[6,7] CNTs might exhibit a rather dispersed range of mechanical properties. Thus it is of fundamental interest to get a better insight into the mechanical properties of CNTs by using a dynamic AFM. Besides this, the use of a CNT as a tip apex possesses several significant advantages: CNTs have a large aspect ratio, allowing various surface structures with steep edges to be readily investigated; because of their large aspect ratio, CNTs have both mechanical strength and a flexible behavior that prevents wear modification of the tube end; and CNTs are chemically low reactive. The two last items, especially, give the invaluable possibility of having a robust AFM tip at disposal that remains unmodified over various AFM measurements. However, when a CNT lies between a tip apex and a surface, resonance frequency shift and damping signal in FM-AFM operation are profoundly modified and should mostly reflect the mechanical response of the CNT. Therefore, it is essential to first use force-gradient spectroscopy by the FM-AFM to understand the oscillation behavior of the AFM cantilever with CNTs prior to any attempt of using CNT for imaging surfaces.

The paper is organized as follows: Section II presents the experimental methodology. After a short description of the experimental procedure, an introduction on continuum mechanics of a beam follows to describe the mechanical response of the CNT, then a variational principle is used to analyze the resonance frequency shifts as a function of the mechanical properties of the CNT. In Sec. III, detailed experimental results under various conditions are presented. Section IV is devoted to the discussion of the experimental results. The discussion contains several items, focusing, in part (also with the help of a FM-AFM virtual machine) on the relationship between damping features and intermittent contact situations in which the free tube end slightly touches the surface.

Beside a general analysis of the resonance frequency shift and damping signal, special care is required to evaluate the influence of the boundary condition describing the contact between the free tube end and the surface. In particular,

asymptotic behaviors corresponding to pinned and free sliding conditions are discussed. Section V is an attempt to use CNT mechanical properties to enhance contrast for AFM images on heterogeneous surfaces.

II. EXPERIMENTAL METHODOLOGY

The MWNT probe (Fig. 1) is fabricated using a technique[5] that ensures firm binding of the MWNT to the AFM tip. The experiments are performed with a Nanoscope Digital Instrument Head NII. Resonance curves of the oscillating cantilever are recorded giving a resonance frequency $\nu_0 = 337.500$ kHz (Appendix B), whereas the spring constant is deduced from the resonance frequency and the known geometrical parameters of the cantilever beam and calculated to be $k_c = 16\ \mathrm{Nm}^{-1}$.

For FM-AFM operation, a sinusoidal excitation is locked at the resonance frequency and the amplitude of the cantilever oscillation is kept constant. The basic principle follows the FM-AFM method[8] using a PLL controller[9] for frequency demodulation. Most measurements have been performed as force distance spectroscopy during the approach and retract of the surface, using a cantilever with an attached nanotube and monitoring the shift of the resonance frequency and variation of the damping. By providing sinusoidal excitation at the resonance frequency, conservative and nonconservative forces can be separated unambiguously.[10–12] In addition, when the oscillation amplitude is kept constant, the damping signal contains information on the additional losses of energy per period due to tip sample interaction.

In Secs. II A and II B we introduce a few mathematical expressions that are of some use for the analysis of the experimental data. Following a number of previous experimental and theoretical works, equations derived from differential geometry are well adapted to describe the elastic behavior of wires with diameters of nanometer size and, in particular, for CNT.[13–15] This introduction aims at showing the influence of the boundary conditions on the mechanical responses of the CNT. Then, a method based on the variational principle of least action,[11,12,16–18] is introduced to analyze the resonance frequency shifts as a function of the mechanical properties of the CNT.

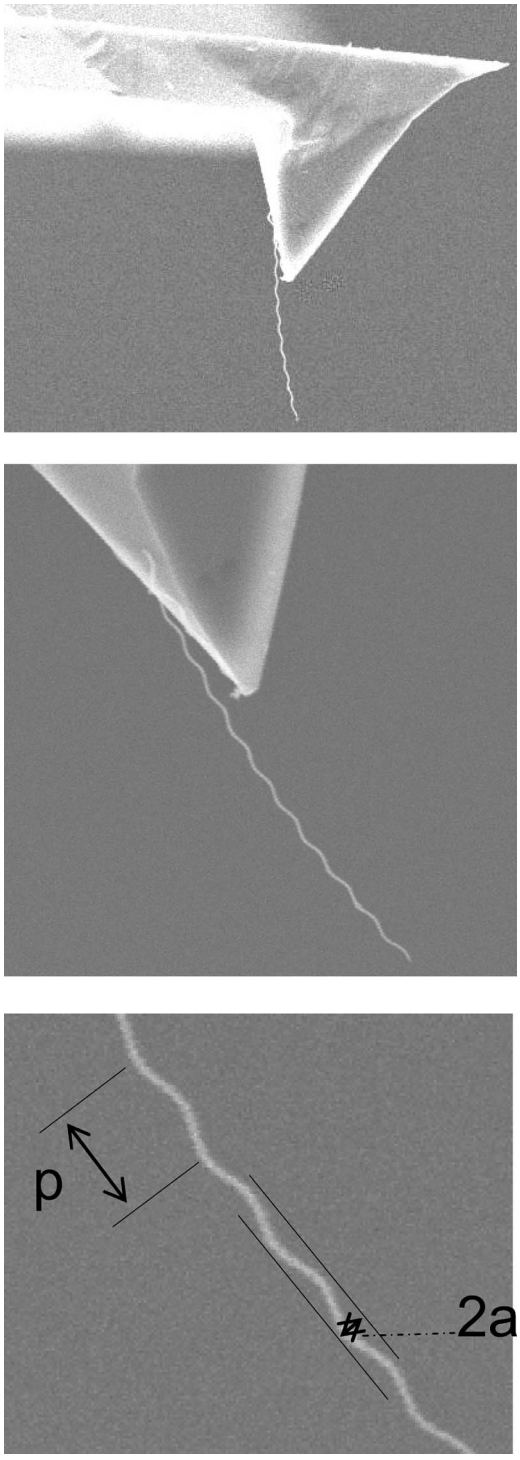

FIG. 1. Scanning electron microscopy image of the Si cantilever tip with a sealed helicoidal C-MWNT. The MWNT used for this study has a free length of about 12 μm, pitch length p of $\sim$1.2 μm, and radius a of $\sim$80 nm.

A. Mechanical properties of a CNT squeezed between a tip and a surface

Although the Young modulus of CNT can be as high as $E = 10^{12}\ \mathrm{Nm}^{-2}$, when these tubes are long and thin, they can become very flexible with a low bending spring constant. To simplify the discussion, consider a tube, which in its undeformed state is a straight cylinder. The tube is squeezed between the tip and the surface, and, when the surface is moved toward the tip, the elastic deformation is first described without considering the helix structure (Fig. 2). In other words, when we restricted ourselves to deformation only involving the symmetry axis of the coiled tube, we consider that the helical structure has a large spring constant so that the shape remains unmodified under the applied external force.

The equilibrium state of a straight tube corresponds to a radius of infinite curvature. If $R(s)$ denotes the radius of curvature at curvilinear coordinate s after an external force has been applied, the elastic bending energy is[19]

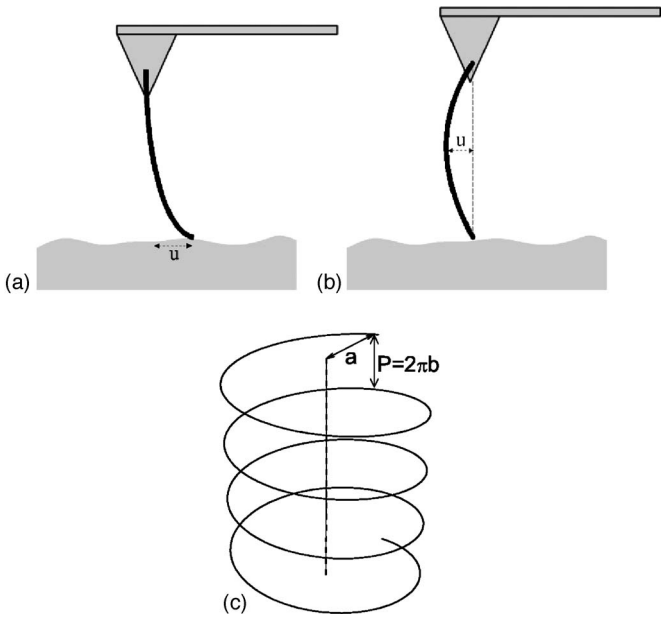

FIG. 2. Scheme of CNT deformation in free-sliding (a) and pinned condition (b). The displacement of the tube u shown in (a) and (b) corresponds to Eqs. (A1) and (A11). The helix parameters P (pitch length) and a (radius) are illustrated in (c).

$$E_{CNT} = \frac{1}{2} EI \int ds \left(\frac{1}{R(s)} \right)^2, \tag{1}$$

where I is the momentum of inertia of the tube section (for a tube of radius r, $I = \pi r^4/4$) and the integration is done over the contour length L. When considering a vertical displacement z, when the CNT end slides free on the surface, the vertical displacement leads to the same lateral displacement [Fig. 2(a)]. Then, with $\boldsymbol{l}(s)$ the vector location of a point on the cylinder, the curvature of the tube is $1/R(s) = d^2\boldsymbol{l}/\mathrm{d}s^2 \sim 2z/L^2$, so that

$$E_{CNT} = \frac{1}{2} E \frac{\pi r^4}{4} L \frac{4z^2}{L^4}. \tag{2}$$

Equation (2) can be rewritten with an equivalent spring constant $\frac{1}{2} k_B z^2$ and leads to the bending spring constant

$$k_B = E \pi r^4 / L^3. \tag{3}$$

Thus, for long CNT (see Fig. 1), the bending spring constant is around 10^{-4} Nm^{-1}, a spring constant several orders-of-magnitude smaller than that of the cantilever.

On the other hand, the spring constant corresponding to tube elongation is much harder than the bending spring constant. The spring constant k_e corresponding to tube elongation is

$$k_e = E \pi r^2 / L. \tag{4}$$

The ratio between the two springs scales as $k_e/k_B \sim (\mathrm{L/r})^2$, and with $r = 40$ nm and $L = 10^4$, k_e is five orders-of-magnitude larger than k_B.

For a tube pinned on the surface and assuming a vertical displacement z inducing a lateral displacement on the midpoint of the tube [Fig. 2(b)], then for small bending deformation so that no buckling instability occurs,[19] the spring constant k_p scales as

$$k_p = \frac{192 EI}{L^3}, \tag{5}$$

which is 64 times larger than the bending spring constant k_B. However, rather than having a clamped condition at both CNT ends, a more appropriate description would be to consider the free tube end pinned on the surface, thus leading to a spring constant smaller than the one calculated with the Eq. (5). Also, it is worth noting that the present analysis does not consider the angular value θ between the cantilever and the surface, nor a possible angle between the tip and the CNT. An angular deviation will give a correction term that may reduce the curvature of the CNT as a function of the vertical surface displacement.

Also for very long CNT, it may happen that only a fraction of the tube is involved in the elastic force, so that the effective contour length one has to use in Eq. (3) might be smaller than the one observed (Fig. 1). Since the spring constant has a cubic power-law dependence on the contour length, any change of the effective contour length leads to significant variations on the spring constant.

For the helical structure one has to evaluate the spring constant associated with elongation of the pitch length. Using usual differential geometry, a helix structure is defined with its radius a, the pitch length $P = 2\pi b$, and the contour length of a helical turn $2\pi(a^2+b^2)^{1/2}$ [Fig. 2(c)]. Consider a deformation of the pitch $2\pi(b+\delta b)$ that does not change the contour length. The force required to stretch one turn of the coil is $k_H 2\pi \delta b$, with k_H given by[20]

$$k_H = \frac{r^4}{8} \frac{E}{(a^2+b^2)^{3/2}} \frac{b^2}{a^2}, \tag{6}$$

where the contribution of the shear modulus has been neglected. The helicoidal shape corresponds to $r = 40$ nm, $a = 80$ nm, and $b = 180$ nm (Fig. 1). For a helicoidal structure, such as the one we have studied, the elongation spring constant remains very large because the pitch length is much greater than that of the radius of the helices. With $L = 10^4$ nm, k_H is nearly equal to the spring constant elongation k_e, then k_H is 4–5 orders-of-magnitude larger than k_B.

In Sec. II B, we turn to a discussion on the way to access the mechanical response of the CNT with the FM-AFM method.

B. Relationship between CNT mechanical responses and resonant frequency shifts

The schemes shown in Fig. 2 represent the basic contributions of the tube elasticity when approach and retract curves are performed. In spite of the simple description of the tube's elasticity, the experimental setup corresponding to a tube squeezed between a tip and a surface might lead to a complex elastic response with a combination of spring con-

stants ranging from $10\ \mathrm{Nm}^{-1}$ to $10^{-4}\ \mathrm{Nm}^{-1}$. For further analysis, we assume that the elongation spring constants or, in general, spring constants much larger than the bending one only contribute during the unsticking of the free end of the CNT from the surface. Therefore, one expects a noticeable contribution to resonant frequency shifts with a frequency jump when the transition to permanent contact situation takes place.

In addition to that, the effective force gradient varies as the intermittent contact increases over an oscillation period. Assume that the type of tube deformation always remains the same over the whole domain of intermittent contact situations, then only one effective spring constant is involved in the frequency shift. When the tube deformation is given by the distance between the tip and the surface, the relative resonance frequency shift is (see Appendix A)

$$\frac{(\nu-\nu_0)}{\nu_0} \approx \frac{1}{2}\frac{k_{NT}}{\pi k_c}(d\sqrt{1-d^2} - \arccos(d)), \tag{7}$$

where k_{NT} is the effective nanotube spring constant. Equation (7) is derived using a variational principle (Appendix A), where d is a reduced coordinate, and is the ratio of the vertical displacement and of the oscillation amplitude.

When the free CNT end is permanently touching the surface, corresponding to $d=-1$ in Eqs. (7) and (A7), the expression between k_{NT} and the resonance frequency shift simplifies

$$\Delta\nu = \nu_0\left(\sqrt{1+\frac{k_{NT}}{k_c}} - 1\right). \tag{8}$$

The low value of the bending spring constant requires the capability to measure the force gradient around $10^{-4}\ \mathrm{Nm}^{-1}$. Such sensitivity is readily obtained with a FM-AFM using a cantilever with a spring constant of $10\ \mathrm{Nm}^{-1}$. With a cantilever spring constant $k=10\ \mathrm{Nm}^{-1}$ and a force gradient of $10^{-4}\ \mathrm{Nm}^{-1}$, one only needs to detect a relative resonance frequency shift of 5×10^{-6}. For a resonance frequency of about 300 kHz, the corresponding shift is about 1.5 Hz and can be measured with commercially available frequency demodulators.[9,21]

When the tube permanently touches the surface, the effective force gradient produces a constant resonant frequency shift [Eq. (8)], which, in the present experiment, is a spring constant or a combination of spring constants. Therefore, even when a simple linear elastic behavior is considered, the mechanical response of the squeezed tube can lead to complicated variations of the force.

Another difficulty that can obscure the analysis of the experimental data is when the tube deformation is no longer proportional to the vertical displacement of the surface. In that case Eqs. (7) and (8) are not valid. However, there is a rather simple way to discriminate situations where the elastic deformation either is or is not proportional to the vertical displacement. Equations (7) and (8) indicate that resonance frequency shifts are independent of the oscillation amplitude. This result is only valid when the tube deformation follows Eq. (A1). When the elastic deformation does not have a linear dependence, the resonant frequency shifts depend on the oscillation amplitude. For example, for an elastic deformation being a square-root function of the distance between the tip and the surface, the frequency shift is (see Appendix B)

$$\frac{(\nu-\nu_0)}{\nu_0} \approx \frac{l}{A}\frac{k_{NT}}{\pi k_c}\sqrt{1-d^2}. \tag{9}$$

In addition to conservative forces of the tip sample interaction, one must also consider dissipative interactions, which give rise to additional energy losses during each oscillation period. Dissipation manifests itself as a hysteresis of the force versus displacement curve. Dissipation mechanisms may involve electrical losses, time delays (as happens in viscoelastic materials[12]), or mechanical instabilities because of adhesion.[11]

The discrimination between the contribution of viscous processes and mechanical instabilities to energy loss might be sometimes difficult to achieve. However, several features are specific to each mechanism. Energy loss because of viscous effects exhibits oscillation amplitude dependence and, when soft materials are involved, an indentation depth dependence.[12] For adhesion hysteresis without any viscous effect, an instability criterion governs the energy loss,[22] and thus must exhibit a threshold value during the vertical displacement that depends on the CNT stiffness and geometry of the contact. Consequently, the damping signal will not show monotonous tip surface distance dependence.

To summarize, Sec. II emphasizes the influence of the interaction between the free CNT end and the surface. The boundary conditions between the free CNT end and the surface can vary significantly from a free sliding condition to a sticking one. Then, different types of contact between the CNT and the surface will lead to different mechanical responses of the squeezed tube as a function of the vertical displacement of the surface. An immediate consequence is that a more or less complex resonant frequency shifts and damping signal evolution will be observed.

For a more systematic analysis, as it is necessary to understand the behavior of the nanotube, one way to vary the boundary conditions is to use different types of surface and to modify the environmental conditions.

III. EXPERIMENTAL RESULTS

Experiments were recorded on silica and graphite surfaces in air. Studies at different pressures were performed from 0.1 mbar up to ambient pressure on silica surfaces. The approach-retract curves are classified into two categories, either ones in which the vertical displacement is large, over several micrometers, or other ones corresponding to small vertical displacements of a few tens of nanometers. The later curves focus on the very beginning of the curves, for which the transition between intermittent and permanent contact situations is investigated, whereas the first ones deal with the competition between adhesion and elastic energy stored in the squeezed tube when permanent contact situations take place.

The experimental results presented are robust and reproducible. However, over several hundred measurements, from time to time some dispersed experimental results were ob-

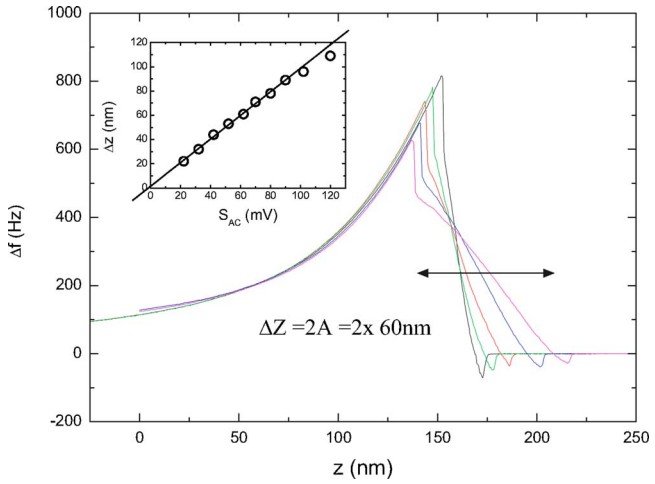

FIG. 3. (Color online) Frequency shift of approach curves on Si measured for different oscillation amplitudes A from 10 to 60 nm. The arrow indicates the intermittent contact region ΔZ for the largest oscillation amplitude, which is twice the oscillation amplitude A. The inset shows the linear increase of the width of the intermittent contact region as a function of the photodiode AC signal S_{AC} proportional to the oscillation amplitude A (see text).

tained. A reasonable hypothesis that can explain change of the curves shape is to invoke variation of the boundary conditions between the free CNT end and the surface, either because of local roughness or heterogeneous chemical properties on the surface.

A. Silica surface

1. Approach curves over short vertical displacement: Effect of the intermittent contact between the CNT and the surface

When performing approach curves on silica surfaces, the resonant frequency shifts first show a decrease then a gradual increase, as depicted in Fig. 3. These common features have been measured for different oscillation amplitudes A. At the beginning of the curve, the resonant frequency decreases within a small vertical displacement of 1–2 nm. The magnitude of the negative shift depends on the oscillation amplitude (Fig. 3). As expected, when the oscillation amplitude is reduced, the magnitude of the resonant frequency shift is increased.[16–18,23,24] Then, a monotonous increase corresponding to repulsive interaction with growing intermittent contact times takes place.

This part of the variation of the resonant frequency is similar to what is usually observed with the FM-AFM method using a standard Si-tip without CNT. The main difference is that for hard surfaces, such curves can only be recorded over a very narrow range of vertical displacements because the feedback loop is unable to keep the oscillation amplitude constant in the repulsive domain due to the large spring constant of the cantilever itself. In the present situation, the variation of the resonant frequency is related to the interaction between the CNT and the surface. In particular, the repulsive part corresponds to the elastic response of the CNT. Consequently, contrary to what is generally observed for standard cantilevers and tips, when a long tube is fixed at the tip apex, a repulsive regime with positive resonant frequency shifts can be observed over a large domain of vertical displacement.

Besides these general results, there are also more unusual features specifically connected to the CNT behavior. At the end of the monotonous frequency increase, a systematic jump of the resonance frequency occurs. These jumps correspond to a sudden enhancement of the repulsive force gradient. In other words, the influence of another spring constant or a combination of spring constants must be considered to fully describe the elastic behavior of the CNT. Thus, consider a domain with a width defined by the beginning of the curve (when the resonance frequency shift becomes negative) and the vertical location, where the positive frequency jump occurs (Fig. 3). The size of this domain varies linearly with the oscillation amplitude (Fig. 3, inset). More precisely, the domain of monotonous increase corresponds to intermittent contacts and can only be twice the oscillation amplitude. This result is easily verified with an independent calibration. As shown below, with the analytical expression [Eq. (7)] and the numerical simulation (see Figs. 4 and 5 and Appendix A), the variation of the resonance frequency and of the damping in the domain over which the intermittent contact occurs are well defined, and predictions and experimental results show a good agreement. Then, the second frequency jump is related to the transition from intermittent contact to full contact of the nanotube (Fig. 5 and Appendix B). Taking these results into account, the same experimental data are displayed in reduced coordinates (Fig. 6), where the vertical displacement is rescaled with respect to the oscillation amplitude.

Examination of the Fig. 6 immediately indicates two distinct domains in the monotonous frequency increase. One domain, at the beginning of the curves that spans over a vertical displacement corresponding approximately to an oscillation amplitude, can be considered as a unique curve. In this part, leaving aside the negative frequency shift, the main features do not depend on the oscillation amplitude. The second domain corresponds to situation where the shape of the curves, including the jump, depends on the oscillation amplitude.

The whole domain under consideration corresponds to intermittent contact situations, or at the very beginning of the resonance frequency curves, to quasi-non-contact situations. The permanent contact happens after a vertical displacement of twice the oscillation amplitude after the first contact between the free CNT end and the surface.

This simple analysis is readily verified through examination of the corresponding damping curves. The characteristic features of the damping curves are displayed in Fig. 7. Simultaneous to a decrease of the resonance frequency (i.e., in the attractive regime), a sharp increase of the damping is observed. In general, but not always, the damping slightly increases, goes through a maximum (approximately located at a vertical displacement of the surface of about the oscillation amplitude), then slightly decreases again. At the end of the domain, the additional damping abruptly decreases and damping coefficients smaller than the one measured when

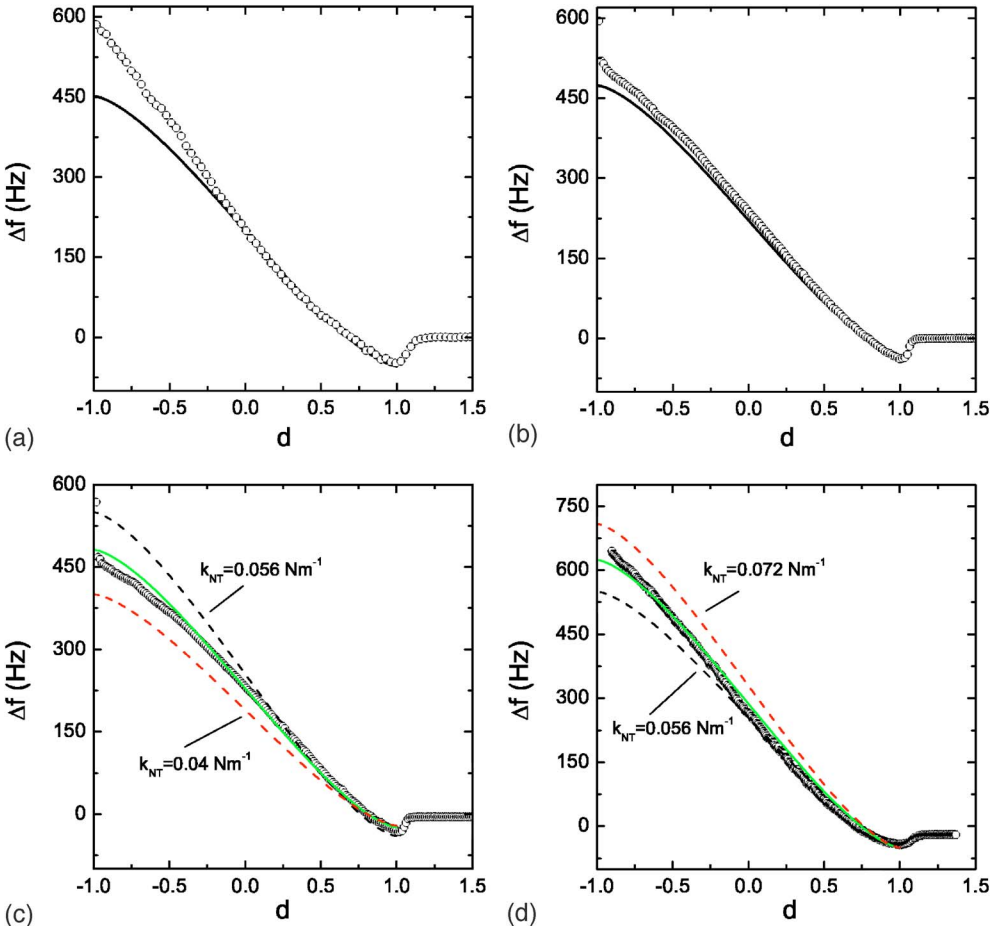

FIG. 4. (Color online) Approach curves on silicon in reduced coordinates $d=Z/A$ (◯) together with calculated curves given by Eq. (7) (continuous and dashed lines) for the intermittent contact region. For (a)–(c) with the oscillation amplitudes $A=15$, 22, and 40 nm, respectively, a value $k_{NT}=0.048$ Nm^{-1} is found; for (d) with $A=42$ nm, the force constant of the nanotube is evaluated to be $k_{NT}=0.064$ Nm^{-1}. (c) and (d) display calculated curves with different spring constants. The comparison indicates the sensitivity on the determination of the spring constant value.

the tip does not interact with the surface can be observed (see Appendix B).

Figure 8 displays the product of the damping signal with the oscillation amplitude. Two different products are reported: the height of the first sudden increase of the additional damping and the maximum damping value at the top of the curve as a function of the oscillation amplitude (see also Fig. 7). From Fig. 8 it can be found that the product calculated from the oscillation amplitude and damping signal at the maximum of the curve varies as a function of the oscillation amplitude, whereas the product of the oscillation amplitude and the height corresponding to the first change of the damping (step height) remains constant. This result means that when intermittent contact situations happen, the dissipative force is mostly a constant, independent of the oscillation amplitude. Furthermore, the abrupt decrease of the damping corresponds to the creation of permanent contact situations between the CNT free end and the surface. All these features indicate that the additional loss of energy is mostly due to adhesion hysteresis occurring with intermittent contact situations. A more detailed analysis of the damping curves, especially of their inner structure, is given in the Sec. IV.

2. Approach curves over large vertical displacement: Influence of the coiled structure

New features are observed when scans with very large vertical displacements are performed (Fig. 9). In the present experiments, keeping in mind a CNT contour length of 10 μm, large vertical displacements mean several micrometers, quite unusual, and very large values in FM-AFM experiments. The resonance frequency shift curves show a sawtoothlike shape, with periodic events of abrupt increase followed by a smooth decrease during the tip approach and, conversely, a smooth increase followed by abrupt decrease during the tip retraction. The distance between two neighboring peaks of resonant frequency shift is about 1.2 μm, which is close to the pitch length of the CNT. Additionally, the same periodicity is observed on the damping curves.

As a first step, the results can be understood as follows: the resonance frequency peaks correspond to a pinned situation of the CNT end, where the elastic energy (which is stored in the tube) becomes too large to keep the pinned situation stable. Thus a competition between the stored elastic energy per unit area of contact and the adhesion energy happens. If the elastic energy per unit area of contact is larger than the adhesion energy (Griffiths criterion, see Ref. 22), the tube starts to slide. The tube slides up to the point at which enough elastic energy is released, then again gets stuck when the next helical turn goes into contact with the surface. Such a sticking-unsticking process, controlled through the competition between elastic and adhesive energy, is common; the less common feature is the periodicity of the process coming from the helicoidal tube shape.

At the end of the sliding motion, there always remains a residual resonant frequency shift increasing monotonously.

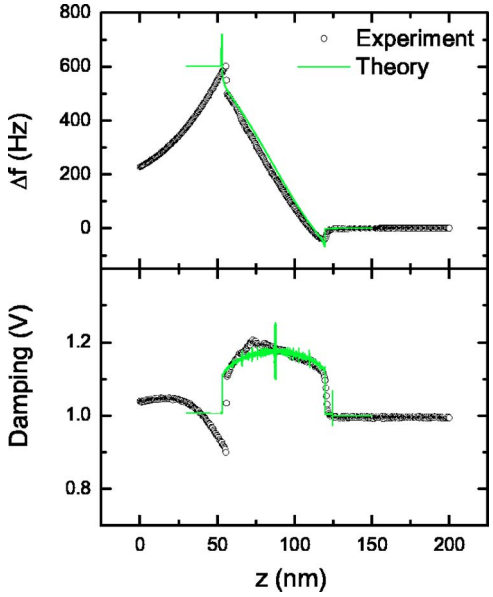

FIG. 5. (Color online) Comparison between a numerical simulation done by using the virtual machine (see Appendix B) and experimental data measured as an approach curve at ambient condition. Top: resonant frequency shift, bottom: damping variation. When using the known parameters of the cantilever (force constant $k=16$ Nm^{-1}, free resonance frequency $\nu_0=335\,000$ Hz, quality factor $Q=500$), the best agreement between theory and experiment in the intermittent contact situation can be found when using a force constant of the nanotube of $k_{NT}=0.044$. Note that the value of the spring constant is close to the one extracted with Eq. (7) (Fig. 4).

The step increase are 14, 41, and 71 Hz for the first, second, and third sliding events, respectively (Fig. 9). With Eq. (3), these frequency shifts lead to the spring constants 1.4×10^{-3}, 3.9×10^{-3}, and 6.7×10^{-3} Nm^{-1}. One may try to address these frequency shifts to spring constants connected to

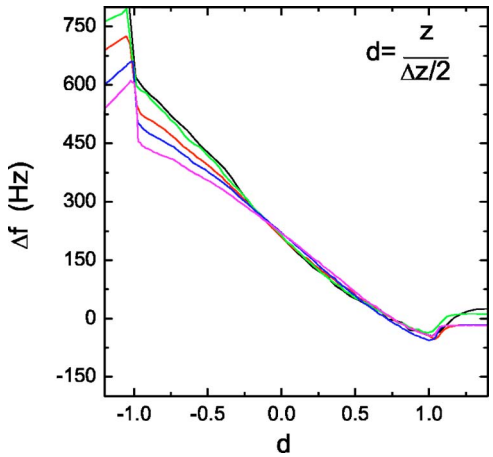

FIG. 6. (Color online) Frequency shift of the approach curves shown in Fig. 3 displayed in reduced coordinates d according to the oscillation amplitudes between 10 and 60 nm. The amplitudes have been derived from the width of the intermittent contact regime in Fig. 3. Offsets have been added to the resonance frequency shifts in order to compensate for the amplitude-dependent sensitivity to attractive forces.

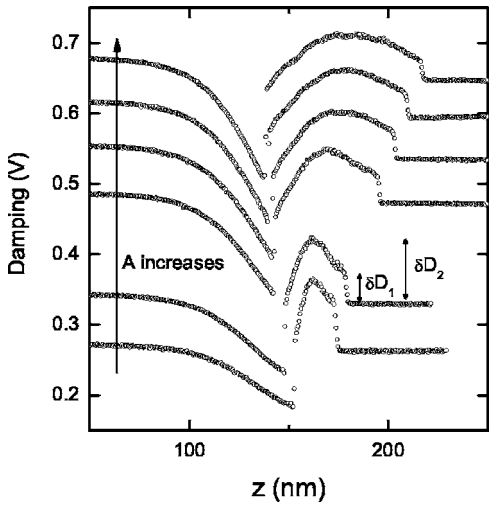

FIG. 7. Damping of typical approach curves on Silica measured for different oscillation amplitudes between 10 to 60 nm. δD_1 and δD_2 indicate the first and second step height of the damping as discussed in Sec. IV.

specific tube deformations. Assuming, that the tube bends with an effective total contour length reduced of one pitch length at each step, and following Eqs. (3) and (8), the remaining frequency shift should increase. However, the cubic law dependence [Eq. (1)] gives a sequence of 14, 22, and 41 Hz, much smaller than the observed sequence of frequency shifts. Several reasons may explain the difference. First of all, values of the first resonance frequency shift show significant variation and, in some circumstances, unexpected nega-

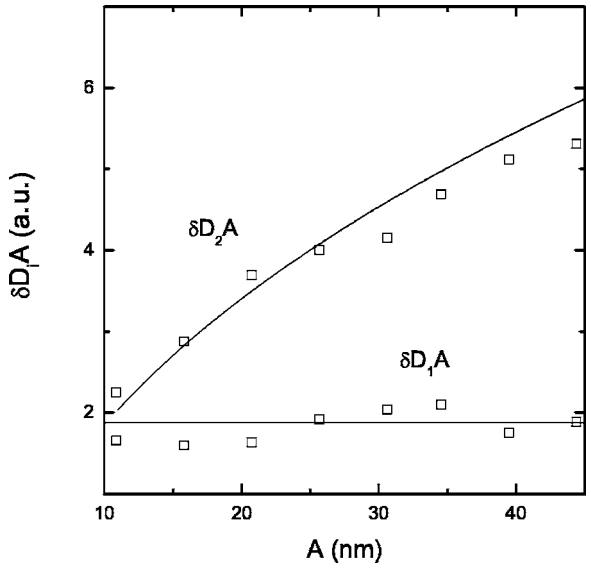

FIG. 8. Variation of the product of the oscillation amplitude A and the additional damping signal δD_i as a function of the oscillation amplitude, where the product $\delta D_i A$ is proportional to the additional dissipated energy. δD_1 corresponds to the first variation at the beginning of the intermittent contact situation, and δD_2 corresponds to the maximum of the damping during the intermittent contact situations (see also Fig. 7 for definition). The continuous line corresponds to the power law A^{α}, where the exponent α is 0.4.

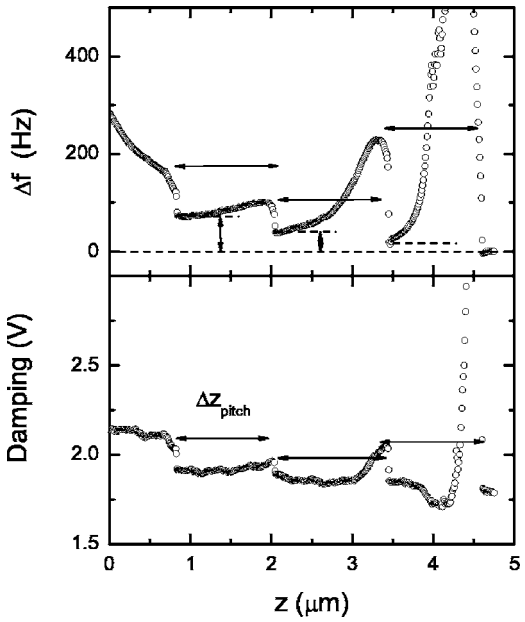

FIG. 9. Resonance frequency shift and damping of an approach curve on Si using the helicoidal MWNT with a large vertical displacement of several microns. Both, frequency shift and damping show a periodic behavior with a characteristic length Δz_{pitch} close to the pitch length P of the coiled nanotube. Small vertical arrows show the residual frequency shift after tube sliding.

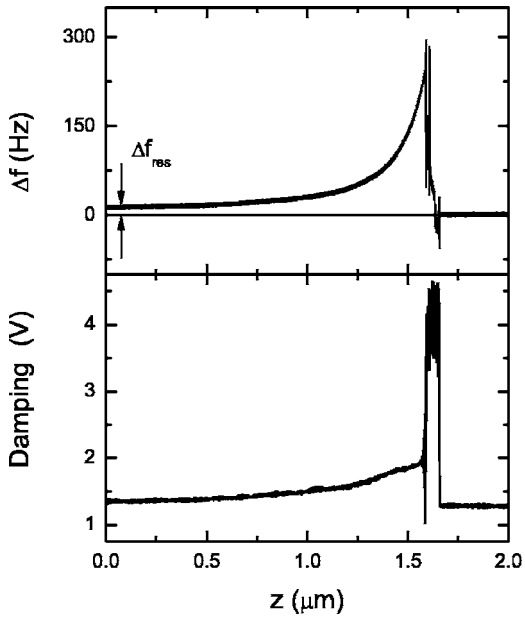

FIG. 10. Frequency shift and damping measured for an approach curve on Si at reduced pressure of about 20 mbar. The residual frequency shift Δf_{res} in full contact situation is about 14 Hz and can be used to calculate the bending force constant k_{Bend} under free sliding conditions.

tive shifts. As a consequence, small values of the frequency shift are not very reliable when large vertical displacements are involved. In particular, the presence of a fluid gas squeezed between the cantilever and the surface contributes to change of the resonance frequency shift. Hydrodynamic forces do not vary significantly when only vertical displacements of a few nanometers are used, but this is not the case when displacements of several micrometers are performed. To address this point, the tube's response was additionally investigated in an environment with rarefied fluid.

B. Low-pressure measurements on silica

The experiments presented in the following section were performed between atmospheric pressure and 1 mbar. The residual resonant frequency shifts were always positive and, in general, larger than that at atmospheric pressure. Typical values were around 10–15 Hz [Fig. 10(a)], corresponding to spring constants of $1\text{–}1.5\times10^{-3}$ Nm^{-1}. Another significant result is the damping evolution with pressure (Fig. 11). Previously, we note that the product of damping with the oscillation amplitude, at least the first step height, does not depend on the oscillation amplitude and that damping disappeared as permanent contact takes place. These two results strongly support a damping mostly governed by the adhesion hysteresis. As shown in Fig. 11, experiments at low pressure also indicate that the additional damping because of the hysteresis of adhesion does not depend on the pressure, whereas the damping of the cantilever, when the tube is far from the surface, shows the usual square-root pressure dependence as expected from damping due to a surrounding viscous fluid.[26] Therefore, within the domain of pressure investigated, the contact between the free CNT end and the surface is not significantly modified.

The other result concerns the abrupt decrease of the damping on transition from intermittent to permanent contact situations [Figs. 9(b), 10(b), and 12]. As already noted (see

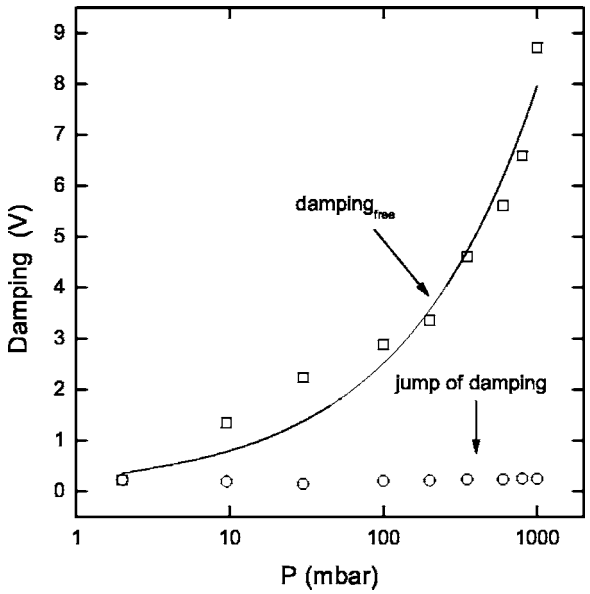

FIG. 11. Evolution of the free damping value, when the tube does not touch the silica surface (□), and the first jump of the damping (◯) both as a function of the gas pressure. As indicated by the continuous line, the free damping value shows a square-root-like increase with the pressure p, while the first jump of the damping remains constant as a function of the pressure P.

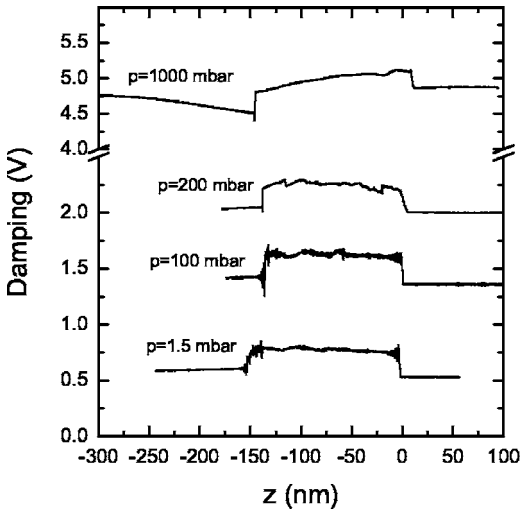

FIG. 12. Evolution of the damping as a function of the pressure. The negative variation of the damping observed at atmospheric pressure disappears when the pressure is lowered.

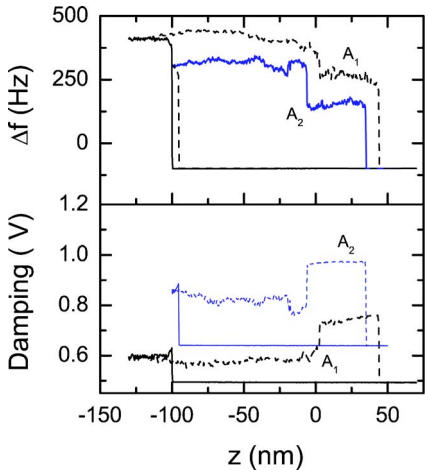

FIG. 13. (Color online) Two approach retract curves measured on graphite at different oscillation amplitudes $A_1=25$ nm and $A_2=35$ nm. In both cases, a large hysteresis of ~150 nm (A_1), respectively, ~130 nm (A_2) is observed. Prior to the jump, during the approach (solid line) no detectable events are observed. During the retraction (dotted line), damping jumps correspond to abrupt decreases of the frequency shift, then the damping remains at the higher value before the CNT leaves the surface.

also discussion in Sec. IV), for the permanent contact situation, the additional damping due to adhesion hysteresis should disappear. However, at atmospheric pressure, this abrupt variation often leads to a negative variation of the damping. A damping lower than the one measured when the CNT end does not interact with the surface is surprising and not related to physical properties of the CNTs. As can be seen from Fig. 10(b), the negative variation reduces as the pressure decreases and becomes almost not measurable below 600 mbar (see Appendix B). Figure 10(b) shows the abrupt decrease of damping at the transition to full contact and then a slow, monotonous, reduction toward the initial value of the damping signal. This evolution is in agreement with the interpretation of a final free sliding situation in which variation of the contact area between the tube and surface has a negligible influence.

As emphasized in Sec. I and in agreement with the present experimental results, the type of contact between the CNT and the surface can profoundly modify the magnitude of the spring constant [see Eqs. (3)–(5)]. Therefore, the use of different surfaces can be a way to investigate different boundary conditions, in turn, to show different variations of the resonant frequency shifts as a function of the surface vertical displacement.

C. Graphite surface

Typical results recorded on the graphite surface are displayed in Figs. 13 and 14. The curves show two astonishing results. First, there is no negative frequency shift related to an attractive interaction and second, there is no evidence of intermittent contact situations. Instead, at low and intermediate oscillation amplitudes the approach curves show a steplike increase of the resonance frequency shift of several hundred hertz [Fig. 13(a)]. Therefore a completely different variation of the frequency shift is founded. In the following, through an investigation of the experimental results, we shall try to extract a qualitative picture to better understand the absence of negative frequency shifts and the absence of intermittent contact situations.

The absence of negative frequency shifts can be understood as a consequence of an attractive interaction too weak to be detected. The absence of intermittent contact situations is more difficult to understand. Before the tube reaches a permanent contact situation we necessarily investigate a situation where an intermittent contact must occur. As predicted with Eq. (7) and shown with the experimental data recorded on the silica surface, change on intermittent contact situations leads to change on the resonant frequency shift. Therefore, on the contrary, to a steplike behavior, one should first observe a continuous increase of the positive frequency shift.

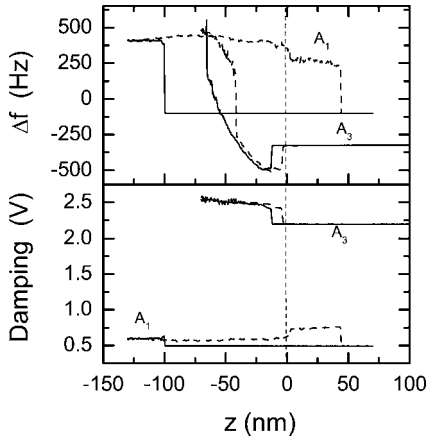

FIG. 14. Resonance frequency shifts and damping variations as a function of the vertical displacement on graphite for two oscillation amplitudes of 25 nm (A_1) and 195 nm (A_3). As shown with the retraction curve, when the amplitude A_3 is used, the oscillation amplitude becomes large enough to unstick the remaining glued part of the CNT.

In addition to resonance frequency jumps, damping jumps are also observed at the same vertical location [Fig. 13(b)], but no events were observed before the jump. Thus, there is no evidence of interaction between the tube and surface prior to this jump. Therefore, if any contact occurs at a vertical location before the observed damping and frequency jumps, as it should be, the interaction between the free CNT end and the surface and also the CNT elastic deformation must be too weak to be measured.

Examination of the retract curves and use of greater oscillation amplitudes provide additional information, showing that part of the tube was already lying on the surface before jumps of the frequency and damping occur.

At low and intermediate oscillation amplitudes retract curves give unusual large hysteresis on frequency shifts and damping with a size of typically 200 nm [Figs. 13(a) and 13(b)]. This large cycle suggests that during the approach the tube was, in part, over a length of $\sim$100 nm already sliding on the surface. Since neither frequency shift nor damping was observed, such a contact corresponds to the free sliding condition with negligible elastic deformation of the tube. During the retraction, another noticeable event is the abrupt decrease of the frequency accompanied of a corresponding increase of the damping. Following our previous analysis of a damping mostly connected to adhesion hysteresis during intermittent contact situations, the present accident indicates that part of the tube, now stuck and unstuck over the oscillation period, before it completely leaves the surface. When larger oscillation amplitudes are used, the remaining part of the glued tube is removed [Figs. 14(a) and 14(b)].

These experimental results indicate the intricate relation between the resonance frequency shifts, which are used to obtain an image, and the interaction between the CNT and the surface. Section V will be specifically dedicated to the use of the MWCNT to vary the height contrast of an image.

IV. DISCUSSION: MODELING THE CNT MECHANICAL PROPERTIES

A. Tube deformation and spring constants

A simple way to start the analysis of the experimental data is an attempt to assign the observed frequency step heights to spring constant values. Using Eq. (8) with a resonance frequency of 337 kHz and a cantilever stiffness $k=16$ Nm^{-1}, a frequency shift of 500 Hz, a typical value observed on graphite, gives a CNT spring constant of 4.5×10^{-2} Nm^{-1}. On silica surface in rarefied air, the remaining frequency shift observed when the tube slides is 10–15 Hz (Fig. 10). Thus, the corresponding spring constants are about 1–1.5 $\times10^{-3}$ Nm^{-1}. For silica surfaces, the low values of the spring constant suggest that the frequency shifts are related to bending deformation of the CNT. For graphite surfaces, a much larger frequency shift can be explained with the fact that a significant part of the tube is already lying on the surface, thus leading to a larger spring constant when the tube end firmly sticks on the surface.

Now consider the frequency shift curves with intermittent contact situations on silica, from which we may expect to discriminate the influence of the different spring constants. We further assume that the elastic deformation is given by the vertical displacement of the surface [Eq. (A1)]. At a given value of the reduced distance d, the frequency shift remains the same, whatever the oscillation amplitudes used (Fig. 6). Therefore, Eq. (7), predicting that the resonance frequency shifts do not depend on the oscillation amplitude for intermittent contact situations, should be able to satisfactorily fit the common part of the curves displayed in Fig. 6. In order to get better insight on the use of Eq. (7), theoretical curves are separately compared to the experimental ones (Fig. 4). Equation (7) gives good agreement on the overall frequency shifts. A fit procedure gives a spring constant $k_{NT}=4.8\times10^{-2}$ Nm^{-1} [Figs. 4(a)–4(c)], an order-of-magnitude larger than the spring constant deduced from the step height frequency variation when the CNT slides. The result is robust since similar experiments repeated from time to time give a spring constant close to that one. As an example another comparison is shown in Fig. 4(d), where the fitting parameter leads to spring constant $k_{NT}=6.4$ $\times10^{-2}$ Nm^{-1}. Figures 4(c) and 4(d) present several calculated curves using different values of the spring constant. Thus, as shown with this comparison, although the spring constants remain close, the difference is fully significant, indicating a change in the contact between the tip and the surface. Beyond the point where the curves are no longer identical (see Fig. 6), expression (7) becomes unable to describe the evolution of the resonance frequencies. The noticeable difference is an unambiguous influence of the oscillation amplitude on resonance frequency shifts. As predicted with Eq. (9), an oscillation amplitude dependence on the resonance frequency shift may indicate that the tube deformation is no more a simple linear function of the vertical displacement.

Consider, that only a bending deformation contributes when the tube slides, then the residual frequency shift of 10 Hz gives a force gradient of 10^{-3} Nm^{-1} and Eq. (3) gives a Young's modulus $E\sim10^{11}$ Nm^{-1}. This value suggests that the tube is mostly curved with an almost free sliding situation. For intermittent contact situations the spring constant increases of about a factor 20–30. This result suggests that the force variation is now due to tube deformation, for which the CNT end hardly slides on the surface. In agreement with the predicted variations of the spring constants for the different types of tube deformation [Eqs. (3)–(6)], these values show how much the tube parameters are connected to the type of contact between the tube and surface. Analysis of the corresponding damping curves leads to identical conclusions (see Sec. VI).

Further vertical displacements, with a tube permanently touching the surface, lead to a decrease of the frequency shift with a power law that does not depend on the oscillation amplitude. This result strongly supports the interpretation that the tube starts to slide with a tube deformation becoming again proportional to the vertical displacement. In other words, the strength of the pinned end becomes less efficient, leading to a main contribution of a bending spring constant with a progressive extension of an effective tube length involved in the elastic deformation [see Eq. (3)]. Consequently, the whole variation of the resonance frequency can be summarized as follows: at the beginning of the resonance fre-

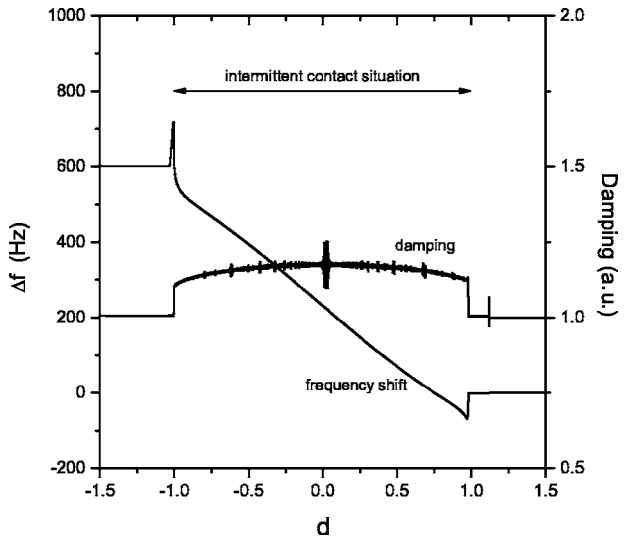

FIG. 15. Typical results obtained with the virtual machine showing the unambiguous relation between intermittent contact situation and additional damping as a function of the reduced coordinate *d*.

quency curve, the attractive interaction dominates, in general, within a small range of vertical displacement of ~1 nm; then the intermittent contact situation leads to a rather large force gradient, indicating a combination of different spring constants, however, the tube deformation remains mostly describable with a linear dependence in *Z*. This result suggests that during the intermittent contact situation, a pinned condition is fulfilled. After a squeeze of the tube of about the oscillation amplitude, the contribution of tube deformation that is not proportional to the vertical displacement becomes noticeable, then at the transition point between intermittent contact and permanent contact situation, a frequency jump happens. The whole scenario, except the full contact situation and mixing of sticking and sliding, is reasonably well described with the virtual machine (Figs. 5 and 15). When permanent contact takes place tube compression induces the sliding leading at the end to frequency shift close to the one expected from bending deformation of almost the whole tube.

B. Dissipative forces

Since the observed additional dissipative force is mostly a constant, whatever the oscillation amplitude, the discussion focuses on contribution due to adhesion hysteresis. Because the adhesion hysteresis induces dissipation, one can formally rewrite the adhesion force with an equivalent damping coefficient that contains several harmonics.[11] The damping signal is only related to the first harmonic, then the additional forcing force we need to keep the oscillation amplitude is formally related to the equivalent damping coefficient to its first harmonic. Thus, we can write $f_0=\gamma^0_{\mathrm{int}}\omega A$, with γ^0_{int} the effective damping coefficient, ω the resonant frequency and A the resonant oscillation amplitude. The product $\gamma^0_{\mathrm{int}}A$, where γ^0_{int} is equivalent to the damping coefficient D recorded with the PLL[9] is, within a first harmonic approximation, closely connected to the true energy dissipated. In that case, the dissipative force, or the product $\gamma^0_{\mathrm{int}}A$, is a constant. In Figs. 7 and 12 several variations of the damping are presented. The whole variation of the damping indicates that the additional dissipation is only observed with intermittent contact situations, thus when adhesion force is involved. Adhesion force prevents a free sliding motion of the CNT end on the surface, and the spring constant deduced from Eq. (7) cannot only be connected to true bending deformation but must include some additional higher spring constant contribution. As a result, Eq. (8) and the observed slope of the frequency shift give a spring constant 30 times greater than the one deduced when the tube slides (Figs. 9 and 10).

Because the sudden increase of the damping at the beginning of the curve relies on the attractive interaction, it might be of interest to connect the maximum of the negative frequency shift to the damping height. An attempt to rely the magnitude of the negative resonance frequency shift to damping height is done with the virtual AFM machine. The result of the numerical simulation is displayed in Fig. 5, showing a reasonable agreement between calculations and experimental data. When the tube slides, on the contrary, almost no additional damping is observed [Figs. 9(b) and 10(b)] showing that we do not have adhesion hysteresis or significant friction forces acting on the tube during the sliding.

As noted, for some experiments a slight increase and then a decrease of the damping was observed, with a maximum located on the middle of the curve (Fig. 7). The middle of the curve corresponds to a vertical displacement equal to the oscillation amplitude A, thus at this point the tip velocity is maximum when touching the surface. On the contrary, at the beginning of the curve or at the end when the vertical displacement is close to twice the oscillation amplitude, the tip velocity is zero when leaving the surface. Since the tip velocity v is proportional to the oscillation amplitude, the damping variation suggests a velocity-dependent component to the adhesion force on the contrary to the constant damping value when the tip velocity is zero (Figs. 8 and 12). This result is reminiscent of what was observed on viscoelastic materials,[25] for which the adhesion is $W(v)=W_0(1+v^\alpha)$. An attempt to fit the variation of the maximum of damping gives an exponent close to 0.4.

V. IMAGING A HETEROGENEOUS SURFACE WITH A LONG COILED NANOTUBE

In this part we present an example of application where we can take advantage of the previous analysis and use the tube mechanical properties to enhance contrast between parts of a heterogeneous surface.

At first sight, a long coiled CNT does not seem to be the best candidate to improve AFM imaging methods. However, the present experimental results show how much the resonant frequency shift depends on the contact between the free CNT end and the surface. Therefore, because long CNTs have low spring constants, these very peculiar tips might become efficient AFM tips. In particular, with low spring constants, even slight changes of the contact properties between the CNT and the surface can induce noticeable variations of the resonance frequency shift.

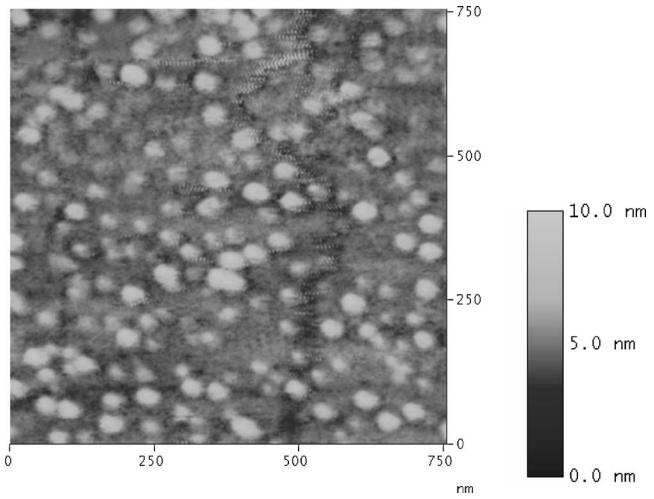

FIG. 16. Height image of the nanodot structure recorded in the repulsive mode using a standard Si cantilever.

The heterogeneous surface chosen for demonstrating the imaging capability is an epitaxial growth of InAs on GaAs substrate. A three-dimensional growing process is obtained, leading to small InAs islands of few tens of nanometers in size. When a usual AFM tip is employed to image the surface, the islands are clearly observed with an average height of 3 nm [Fig. 16]. On contrary, when measuring the same surface with the CNT tip shown in Fig. 1, the InAs aggregates no longer appear as islands, but as holes [Fig. 17]. Thus, the use of the CNT tip leads to a complete opposite contrast between the GaAs substrate and the InAs aggregates, turning the islands into holes.

An appropriate way to understand this reversed contrast is to record variations of the resonance frequency shift as a function of vertical displacement. This has been done by performing approach curves at different *XY* locations—on the GaAs substrate and on the InAs islands.

In Fig. 18 typical variations of the resonance frequency are shown. On the GaAs substrate, the approach curve shows

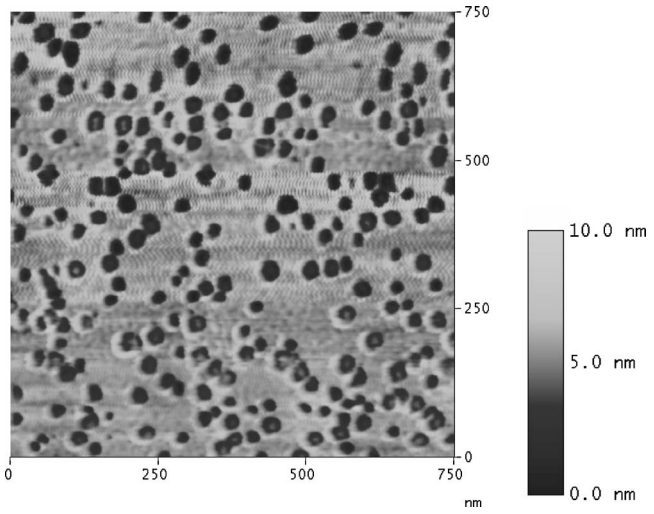

FIG. 17. Height image of the nanodot structure recorded in the repulsive mode using the C-MWNT cantilever.

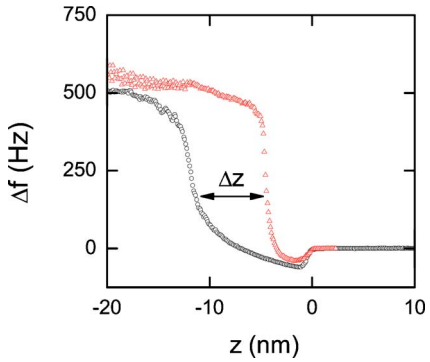

FIG. 18. (Color online) Approach curves on the nanodot structures measured on the dots (○) and beside the dots (△). The distance Δz indicates the difference in vertical displacement (~8 nm) needed to observe the same positive frequency shift of ~150 Hz.

a sharp increase of the resonance frequency shift at a distance <2 nm from the first contact. Compared to what was previously observed, the tip is firmly stuck, leading to an abrupt positive variation of the resonance frequency shift. This result indicates that here the tube deformation corresponds to CNT end pinned on the surface. On the InAs islands the change of the resonance frequency shows a marked difference with a negative frequency shift remaining over a large vertical displacement. Setting the two curves together, the comparison shows a vertical difference of about 8 nm, when a positive frequency shift is employed as a set-point value to control the tip surface distance. Consequently, for the same positive frequency shift used as a set-point value, the piezoactuator moving up and down the surface gives a surface height difference of about 8 nm, which for islands of 3 nm height leads to holes of 5 nm depth (as compared in Fig. 19). The difference explains quantitatively the contrast evolution observed on the image. Therefore the formation of holes corresponds to contact changes of the CNT on the islands with weaker attractive interaction and easier sliding conditions. Besides, in spite of a large tube diameter, a contrast variation is observed within the nanometer scale.

VI. CONCLUSION

This work was an attempt to better understand the behavior of CNT tips and to show, how FM-AFM techniques can be applied to analyze mechanical properties of the nanotube. Additionally, their specific mechanical properties have been used to image heterogeneous surface.

A thorough investigation of the CNT mechanical properties was performed using a FM-AFM with a PLL electronic. One main advantage of using the FM-AFM method is that it allows one to measure and separate conservative and nonconservative forces. In particular, the damping signal contains information on the additional losses of energy per period due to tip-sample interaction. Then, when resonant frequency shifts and damping signals are simultaneously recorded, a coherent picture of the CNT mechanical response is obtained.

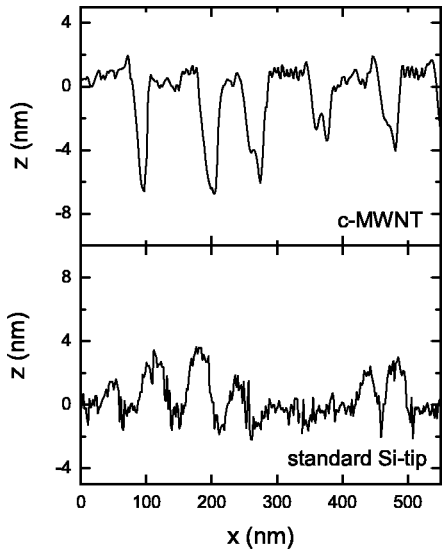

FIG. 19. Cross sections extracted from the images done on the nanodot structures (Figs. 14 and 15). The measurement with the C-MWNT shows the islands as holes (top), whereas the measurement using a standard silicon-cantilever shows them as elevated structures (bottom).

The CNT is firmly stuck on the tip so that the main parameter governing the mechanical response of the tube in interaction with a surface is the contact between the free CNT end and the surface. The variations of the damping signal indicate that additional energy losses are mostly due to adhesion hysteresis. When no significant dissipation takes place, the companion resonant frequency shifts go to small values, whereas when damping signal is high the resonant frequency shift increases, or is also high. The whole variations show how the contact between the free CNT end and the surface modify the tube elastic response and, in turn, the force gradient measured by the frequency shifts. A decrease, or disappearance, of the additional damping corresponds to a free sliding condition of the CNT end on the surface. This results in low spring constant corresponding to rather soft elastic bending deformation. On the contrary, when the CNT is stuck on the surface the spring constant can increase by more than an order of magnitude as it happens within intermittent contact situations.

The competition between the elastic energy stored in the coiled CNT and the adhesion of the CNT on the surface was observed during approach curves with z displacements of several micrometers by a sawtoothlike behavior of the resonant frequency and a period close to the pitch length of the CNT.

Although not quantitative, the cumulate variations of damping and resonance frequency provide a picture accurate enough to explain the effect for imaging and, in turn, find routes to enhance the contrast. In particular, a long nanotube gives low spring constants and thus quite a high sensitivity and contrast in imaging, which is mostly due to force gradients related to changes of the contact between the CNT end and the surface. Another useful result is the abrupt change of the damping connected to intermittent contact situations in which hysteresis of adhesion occurs. Such a damping variation might be a way to get accurate control of the tip surface distance, just by using a light contact of the tube.

As an example, while not being really expected, CNT tip with long coiled tube of contour length more than 10 μm and helical pitch length of 1.3 μm was able to provide robust and well-defined images with an unexpected high lateral resolution.

ACKNOWLEDGMENTS

It is a pleasure to thank Dr. R. Boisgard and Dr. A. Raman for interesting and useful discussions, and Dr. Peter Kailuweit for supplying the nanodot samples. We gratefully acknowledge a financial support from region Aquitaine. D. D. gratefully acknowledges the financial support by Deutsche Forschungsgesellschaft (DFG).

APPENDIX A: CALCULATION OF A RESONANCE FREQUENCY SHIFT INDUCED BY A CNT DEFORMATION

1. Vertical displacement inducing a linear elastic tube deformation

In this section, a variational method is used to calculate the resonance frequency shift in intermittent contact situations due to a CNT deformation squeezed between a hard cantilever and a surface. The CNT free end begins to touch the surface when the distance D between the tip at rest and the surface is the oscillation amplitude A. Assume the CNT behaves as a tube and consider deformation as shown in Fig. 2(a). Consider a linear relationship between the vertical displacement and the tube deformation. Neglecting any deformation of the helix structure, the helical axis deformation is

$$u(t) = A[\cos(\omega t)] - D. \tag{A1}$$

The elastic energy stored in the CNT is

$$E_{el} = \tfrac{1}{2} k_{NT} u^2(t). \tag{A2}$$

During a cycle, the contact time of the CNT free end on the surface is

$$t = \frac{1}{\omega}\cos^{-1}\left(\frac{D}{A}\right). \tag{A3}$$

The action corresponding to the elastic term[25] is

$$S_{el} = 2x\frac{k_{NT}}{2}\int_0^{(1/\omega)\cos^{-1}(D/A)} u^2(t)dt, \tag{A4}$$

writing the reduced coordinate $d=D/A$ and inserting Eq. (A1) into (A4)

$$S_{el} = k_{NT}\,\mathrm{A}^2\int_0^{(1/\omega)\cos^{-1}(d)} [\cos(\omega t) - d]^2\, dt. \tag{A5}$$

The action of the harmonic oscillator without dissipation is[18]

$$S_0 = \frac{\pi m}{2\omega}A^2(\omega^2 - \omega_0^2) \tag{A6}$$

the minimization with respect to A, $[\partial(S_0+S_{el})/\partial A]=0$ gives the expression of the positive resonant frequency shift

$$\frac{\pi m}{\omega}A(\omega^2-\omega_0^2)-\frac{1}{\omega}Ak_{NT}(d\sqrt{1-d^2}-\cos^{-1}(d))=0,$$

$$\frac{(\omega^2-\omega_0^2)}{\omega_0^2}=\frac{k_{NT}}{\pi k_c}(d\sqrt{1-d^2}-\cos^{-1}(d)), \tag{A7}$$

with $\omega+\omega_0\approx 2\omega_0$ Eq. (A7) gives Eq (7)

$$\frac{(\nu-\nu_0)}{\nu_0}\approx\frac{1}{2}\frac{k_{NT}}{\pi k_c}(d\sqrt{1-d^2}-\cos^{-1}(d)). \tag{A8}$$

Note that k_{NT} may have several values (see text)

$$\frac{k_e}{k_{\mathrm{Bend}}}=\frac{E\pi r^2}{L}\frac{4L^3}{3E\pi r^4}=\frac{4}{3}\left(\frac{L}{r}\right)^2\approx 10^5, \tag{A9}$$

$$\frac{k_{\mathrm{Hel}}}{k_{\mathrm{Bend}}}=\frac{Er^4}{8}\frac{b^2}{a^2(a^2+b^2)^{3/2}}\frac{4L^3}{3E\pi r^4}=\frac{1}{6}\frac{b^2}{a^2}\left(\frac{L}{\sqrt{a^2+b^2}}\right)^3\approx 10^5, \tag{A10}$$

with $L=10^4$, $a=80$ and $b=180$ expressed in nanometers.

2. Vertical displacement square-root dependence of the elastic deformation

Again we consider a bending deformation. In place of Eq. (A1), simple geometrical consideration leads to square-root dependence of the tube elastic displacement as a function of the vertical one [Fig. 2(b)]

$$u(t)\approx\sqrt{2l[A(\cos(\omega t))-D]}, \tag{A11}$$

where the length l is the tube contour length that determines the lateral elastic deformation. Inserting expression (A11) in Eq. (A4) and doing the same procedure we get

$$\frac{(\omega^2-\omega_0^2)}{\omega_0^2}=\frac{2l}{A}\frac{k_{NT}}{\pi k_c}\sqrt{1-d^2} \tag{A12}$$

and the frequency shift

$$\frac{(\nu-\nu_0)}{\nu_0}\approx\frac{l}{A}\frac{k_{NT}}{\pi k_c}\sqrt{1-d^2}. \tag{A13}$$

Appendix B: Analysis by using the virtual machine

In order to get a more coherent picture of the response of the system under influence of the hysteresis of adhesion and the elastic response of the nanotube, we have applied the virtual FM-AFM,[15] where the frequency shift and the damping are evaluated by numerical solution of the differential equations describing the oscillation of the tip in the time domain. As the influence of all electronic components is considered together with the physical behavior of the tip-sample system, the virtual machine allows simulating the complete FM-AFM used in this work. In our case, the application of the virtual machine has two main advantages: first, the numerical approach enables us to simulate the amplitude and the damping for even quite complex tip-sample interaction during the oscillation in the intermittent contact situation, and second, the complete description of the AFM with all the accompanying parts helps to separate physical effects from effects induced by the influence of the electronics.

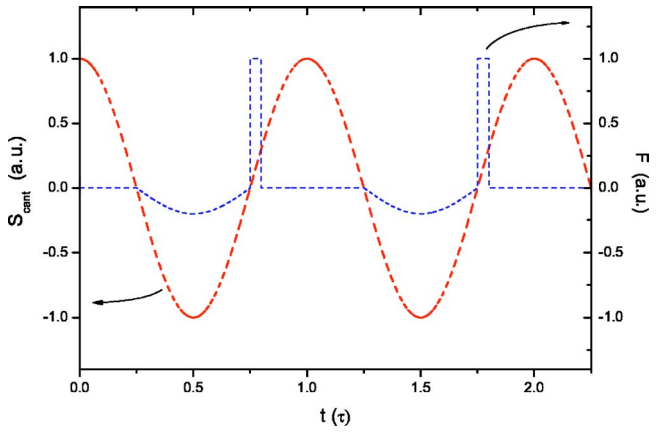

FIG. 20. (Color online) Sketch of the force used for the simulation.

Most of the features observed in the experimental results of the frequency shift and damping during force spectroscopy curves using the CNT cantilevers are described by a comparatively simple model assuming an elastic response of the nanotube and an hysteresis of adhesion of the tip at the surface as it is shown in Fig. 20. When the tip is not in contact with the surface, the force due to the cantilever is zero ($t=0-0.5$ in Fig. 20). When the tip touches the surface, the CNT immediately reacts with a repulsive force proportional to the relative position of the cantilever to the surface. This repulsive force corresponds to a comparatively high force constant k_B related to the bending of the sample due to the firm sticking of the end of the tube to the sample surface. This sticking is also effecting the tip-sample interaction when the tube is removed from the surface ($t=1$ in Fig. 20). During a very short distance a high sticking force is effecting the tube-cantilever system before the tube finally unsticks and the interaction force is zero again.

This shape of force has been used to calculate the frequency shift and the damping during an approach curve in FM-AFM mode (Fig. 15). When the tip is far away from the surface, we obtain a constant frequency shift, related to the force constant of the cantilever itself. At the instant when the cantilever touches the surface we observe a sudden change, both on frequency shift and damping signals. These changes are related to the sudden occurrence of the nonconservative hysteresis of adhesion and the related attractive force during the unsticking process. When the cantilever further approaches the surface, additionally, the repulsive forces due to the bending of the tube have to be considered. These conservative forces do not change the damping but lead to an increase of the frequency shift. The frequency shift continuously increases until the nanotube can no longer become unstuck from the surface. This sudden change again leads to a steplike change of the damping and frequency response of the system, resulting in a decrease of the damping and an increase of the frequency shift. The whole intermittent contact situation has a width of two times the oscillation amplitude and should therefore vary linearly with the amplitude as it has been shown (inset of Fig. 3).

This model has then been used to fit the experimental results (Fig. 5). Although, we see quite a reasonable agreement of the general features, there are still some discrepancies when looking at the details. One deviation between theory and experiment can be found in the beginning of the intermittent contact situation. While the simulation predicts a very sharp decrease of the frequency shift, the experiments show a rather smooth transition. This may be because of two reasons: (i) the attractive van der Waals interaction, which is already affecting the noncontact situation, has not been considered and (ii) the comparatively large diameter of the tube makes it probable that the sticking is not instantaneous, but that the tip is moving into the fully clamped condition within 1–2 nm. The clamped bending force constant, however, is in good agreement with the one determined from analytical calculations [Eq. (A7)].

The damping shows deviations, most probably as the velocity dependence of the unsticking process, which has been found by amplitude-dependent measurements (Fig. 8), has not been considered in the interaction model. The simulation gives a fairly good description of the jump of the frequency shift at the end of the intermittent contact situation and the decrease of the damping. Therefore, the damping conditions seem to be mostly governed by the hysteresis of adhesion. This becomes also clear because the hysteresis of adhesion describes both the magnitude of the negative frequency shift and the increase of the damping at the same time.

A confusing and unexpected result is the occurrence of a negative variation of the damping, leading to damping values smaller than the one measured when the CNT does not interact with the surface. One notes that such a variation occurs when strong interaction takes place with a noticeable resonant frequency shift, furthermore the negative variation disappears as the pressure gas is reduced [see Figs. 12 and 10(b)].

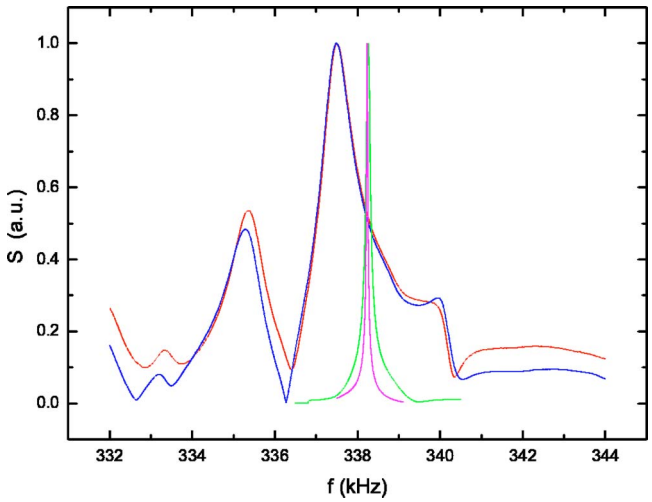

FIG. 21. (Color online) Resonance curves at atmospheric pressure (Q=560), 100 mbar (Q=4230), 1 mbar (Q=14090).

The most reasonable hypothesis relies on the evolution of the resonance curves when the viscous damping is reduced. Because of ill-defined resonance curves at atmospheric pressure (Fig. 21), which is a feature often observed with cantilever having a resonance frequency in the domain 300–350 kHz,[22] a large frequency shift may lead to unusual nonlinear events that disappear when a perfect harmonic oscillator is recovered over a wide range of frequency as it happens at low pressure.

*Electronic address: jp.aime@cpmoh.u-bordeaux1.fr

[1] S. Iijima, Nature (London) **354**, 56 (1991).
[2] H. W. Zhu, C. L. Xu, D. H. Wu, B. Q. Wei, R. Vatjai, and P. M. Ajayan, Science **296**, 884 (2002).
[3] C. H. Kiang, M. Endo, P. M. Ajayan, G. Dresselhaus, and M. S. Dresselhaus, Phys. Rev. Lett. **81**, 1869 (1998).
[4] A. Thess *et al.*, Science **273**, 483 (1996).
[5] C. V. Nguyen, K. J. Chao, R. M. D. Stevens, L. Delzeit, A. Cassel, J. Hans, and M. Meyyappan, Nanotechnology **12**, 363 (2001).
[6] W. Z. Li, S. S. Xie, L. X. Qian, B. H. Chang, B. S. Zou, R. A. Zhao, and G. Wang, Science **283**, 512 (1999).
[7] L. Marty, V. Bouchiat, A. M. Bonnot, M. Chaumont, T. Fournier, S. Decossas, and S. Roche, Microelectron. Eng. **61-62**, 485 (2002).
[8] T. R. Albrecht, P. Grütter, D. Horne, and D. Rugar, J. Appl. Phys. **69**, 668 (1991).
[9] NanoSurf A.G. Easy PLL FM-detector and sensor controller, www.nanosurf.com
[10] J. P. Cleveland, B. Anczykowski, A. E. Schmid, and V. B. Elings, Appl. Phys. Lett. **72**, 2613 (1998).
[11] U. Dürig, New J. Phys. **2**, 5.1 (2000).
[12] R. Boisgard, J. P. Aimé, and G. Couturier, Surf. Sci. **511**, 171 (2002); F. Dubourg, J. P. Aimé, S. Marsaudon, R. Boisgard, and P. Leclère, Eur. Phys. J. E, **6**, 49-55, (2001).
[13] J.-P. Salvetat, A. J. Kulik, J.-M. Bonard, G. Andrew D. Briggs, T. Stöckli, K. Méténier, Sylvie Bonnamy, F. Béguin, N. A. Burnham, and L. Forró, Adv. Mater. (Weinheim, Ger.) **11**, 161 (1999).
[14] S. Cuenot, C. Frétigny, S. Demoustier-Champagne, and B. Nysten, J. Appl. Phys. **93**, 5650 (2003); S. Cuenot, S. Demoustier-Champagne, and B. Nysten, Phys. Rev. Lett. **85**, 1690 (2000).
[15] A. Kis, S. Kasas, B. Babić, A. J. Kulik,[1] W. Benoît, G. A. D. Briggs, C. Schönenberger, S. Catsicas, and L. Forró, Phys. Rev. Lett. **89**, 248101 (2002).
[16] J. P. Aimé, R. Boisgard, L. Nony, and G. Couturier, Phys. Rev. Lett. **82**, 3388 (1999).
[17] U. Dürig, Surf. Interface Anal. **27**, 467 (1999).
[18] L. Nony, R. Boisgard, and J. P. Aimé, J. Chem. Phys. **111**, 1615 (1999).
[19] L. D. Landau and E. M. Lifshitz, *Theory of Elasticity* (Pergamon, London, 1959).
[20] P. Bugl and S. Fujita, J. Chem. Phys. **50**, 3137 (1969).
[21] G. Couturier, R. Boisgard, L. Nony, and J. P. Aimé, Rev. Sci. Instrum. **74**, 2726 (2003).

[22] D. Maugis, Mater. Sci. **20**, 3041 (1985).
[23] F. J. Giessibl, Phys. Rev. B **56**, 16010 (1997).
[24] H. Hölscher, B. Gotsmann, W. Allers, U. D. Schwarz, H. Fuchs, and R. Weisendanger, Phys. Rev. B **64**, 075402 (2001).
[25] J. D. Ferry, *Viscoelastic Properties of Polymers* (Wiley, New York, 1970).
[26] E. O. Tuck, J. Eng. Math. **3**, 29 (1969); J. E. Sader, J. Appl. Phys. **84**, 64 (1998).